Experimental Study on the Characteristics of Liquid Film Driven by High Speed Airflow

Qiyu Shi [1], Shinan Chang [1]*, Mengyao Leng [1]

[1] Beihang University, School of Aeronautic Science and Engineering, Beijing 100083, China

*sn_chang@buaa.edu.cn

Abstract

The characteristics of liquid film driven by high speed airflow were studied experimentally in order to elucidate the underlying physics of the dynamic water runback process pertinent to aircraft icing phenomena. Planar laser-induced fluorescence (PLIF) technique was applied for the visualization and non-intrusive measurements of thin liquid film over a range of film Reynolds numbers Re_f=41-208 and wind speed U_a=10-50m/s. Three flow regimes, named 'two-dimensional wave', 'three-dimensional wave' and 'disturbance wave' regimes, have been identified and characterized based on observation results and processed statistics. Quantitative analysis including the mean film thickness, interface roughness and wave statistics were conducted to provide an insight into the flow structure and microphysics of wind-driven liquid film.

1 Introduction

Aircraft icing occurs when a cloud of supercooled droplets impinge and freeze onto the airplane surface, posing a threat to fight safety. In glaze icing conditions, only a fraction of the collected water freezes in the impingement area and the remaining water runs back forming water film, rivulets and water beads (Olsen and Walker, 1987). The glaze ice has been considered as the most dangerous icing hazards for its complex ice accretion induced by surface water (Gent et al. 2000). A representative ice prediction model, Myers model (Myers and Thompson,1998), has taken into account the runback water film and was widely applied in glaze icing prediction. However, due to the lack understanding of runback water behavior, most of the models apply assumptions and simplifications, which is considered to be a significant factor for the inaccurate predictions (Liu et al.2017). Recently, the development of experimental techniques allows the investigation towards the microphysical characteristics of shear-driven liquid film pertinent to aircraft icing and several investigations have been done. Zhang et al. (2016) applied digital image projection (DIP) technology and demonstrated the phenomena of water film and rivulet formation over an airfoil and a flat plate, respectively. Liu et al. (2017) developed a multi-transducer ultrasonic pulse-echo (MTUPE) technique to quantify the dynamics of the wind-driven water film flows over the test plate. Leng et al. (2018) used confocal chromatic technique to measure the water film thickness and proposed a new correlation of the interfacial shear factor. Cherdantsev et al. (2014) investigated the spatial disturbance wave structure and liquid entrainment phenomena of shear driven liquid film using high-speed LIF technique. Although the above results have contributed to the understanding of wind-driven liquid film, very little can provide quantitative measurements to look deeper into the characteristics. Another limitation is the low speed of certain afore-mentioned experimental airflow for aircraft icing.

In the present study, Planar Laser-Induced Fluorescence (PLIF) technique is applied to achieve non-intrusive thickness measurements of wind-driven liquid film characteristics. The experimental apparatus and measurement method are described in Section 2. The results are demonstrated and analyzed in Section 3 ordered by flow regime and phenomenological observations, film thickness statistics and wave characteristics. Conclusions are summarized in Section 4.

2 Experimental Method

2.1. Experimental apparatus

The experiment setup, as shown schematically in Fig. 1, consists of a small-scale wind tunnel and the measurement equipment. The wind tunnel includes the centrifugal blower, the settling chamber, the contraction section, test section and the diffuser section, with the capable airflow speed of up to 55m/s. The bottom of the test section is equipped with an aluminum test plate with a dimension of 250mm×150 mm and the other three walls of the section are made of Plexiglas to accomplish an omnidirectional perspective of observation. High speed airflow, generated by a centrifugal blower, flows through the test section with cross-section to be 55mm×200mm. A honeycomb and two layers of gauzes are placed in the contraction section to make the generated airflow uniformly flow past the test sections.

The working fluid is injected by a submersible pump, passes through a supplement vessel and then enters the test section though a slot distributor with the width of 8cm to form initial liquid film. The liquid flow rate is measured by pre-calibrated rotameter with an accuracy of 5%. At the end of the test plane, liquid is collected in the collecting vessel through a slot, which is filled with an absorbent sponge material to capture the water and prevent the suction of air. The outlet of the test section is open to the atmosphere.

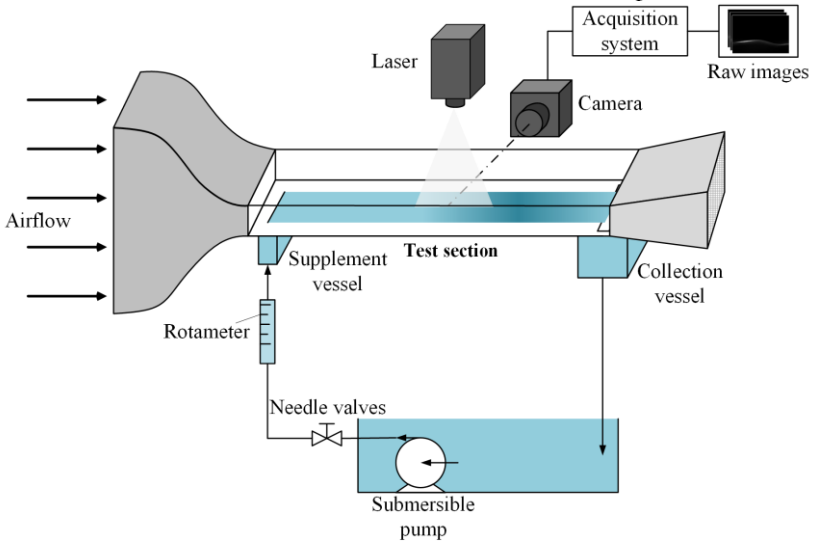

Figure 1: Schematic layout of experimental setup

2.2. Measurement technique

Measurements were performed using a PLIF flow measurement technique, which use a fluorescing material within the liquid phase, a monochromatic laser light, and a camera for observation of the resulting fluorescence (Schubring et al.2010). Current system employed a semiconductor laser with an excitation wavelength of 532 nm. Distilled water doped with fluorescence dye Rhodamine 6G at a concentration of 20 mg/L was used as working liquid. The laser was equipped with sheet optics, with the capability of producing a 0.1mm light sheet for the illumination of working liquid. Since the major emitted light was at the 550nm wavelength, the high-speed camera (Photron FASTCAM Mini UX100) with a 1280×1024 pixel resolution was mounted with a 550nm high-pass optical filter to capture the lighted liquid film. The camera was positioned at 90°to the laser light sheet, 15cm away from the water inlet. The spatial pixel resolution was about 4μm and 5s of instantaneous data was saved with the frame rate of at least 500 Hz.

All the tests were carried out at room temperature and under stationary conditions. The range of airflow speed and film Reynolds number were U_a=10-50m/s and Re_f=41-208, respectively. Re_f is defined as Q/wv_l, where Q, w, v_l denotes the volumetric liquid flow rate, the film width and the kinematic viscosity of the liquid, respectively. All the experiments were carried out after the water film was stabilized.

3 Results and Discussion

The PLIF results are demonstrated in this section to provide an insight into the flow structure of wind-driven liquid film. The raw images are processed by self-developed MATLAB code with the capability of identifying the edge of liquid film and then the film thickness statistics are extracted for quantitative analysises. In section 3.1, temporal film thickness time-traces and several corresponding LIF images are demonstrated for the qualitative analysis of flow regimes and phenomenological observations. Following this, section 3.2 presents the quantitative results on film thickness, interface roughness and power spectral density for better understanding on the underlying physics of wind-driven liquid film.

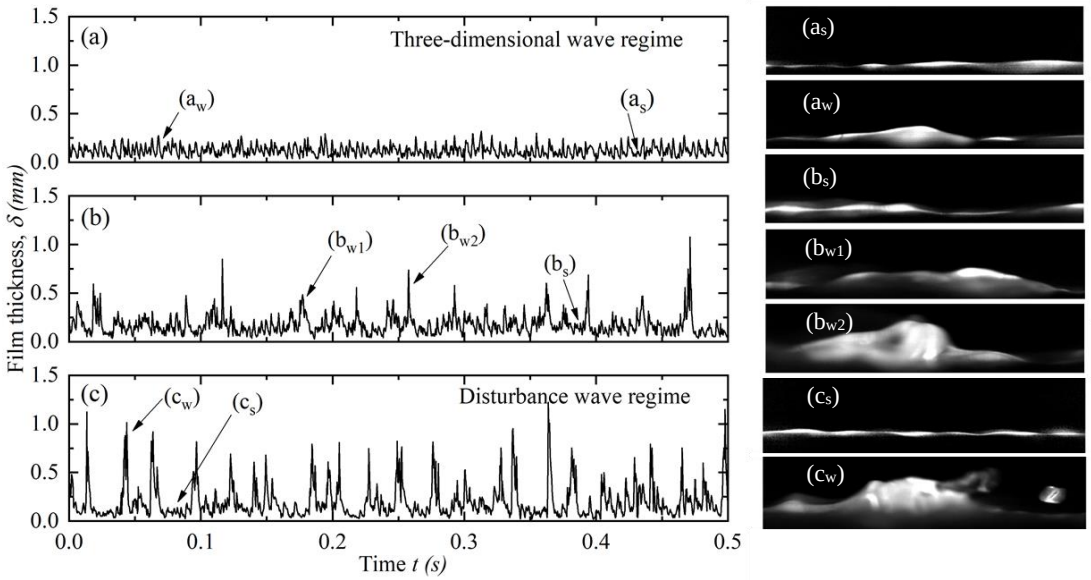

Figure 2: Temporal film thickness time-traces and instantaneous raw PLIF images of wave fronts (χ_w) and substrate (χ_s) for U_a=50m/s and Re_f of: (a) 41, (b) 124 and (c) 207.

3.1 Flow regime and phenomenological observations

Three distinct flow regimes are identified based on experimental phenomena and previous studies. The example of temporal film thickness time-traces and the instantaneous raw PLIF images of wave fronts and substrate for U_a=50m/s and film Reynolds numbers Ref of 41, 124 and 207 are shown in Fig. 2.

(i) 'Two-dimensional wave' regime

The 'two-dimensional wave' regime ('2-D wave' regime) occurs at relative low airflow speed, which was 10m/s for current condition. In general, surface waves of this regime are uniform and periodic with wave crests straightly spanning almost the entire film width, forming a two-dimensional structure. For Re_f below 127, the '2-D wave' regime was dominated by obvious sinusoidal waves with approximately the same wave length. With the increase of the liquid flow rate, the outline of the sinusoidal waves became unsmooth with small ripples generated on the wave crests. Then, the straight leading edge changed into curves and the separated three-dimensional waves occurred.

(ii) 'Three-dimensional wave' regime

The 'three-dimensional wave' regime ('3-D wave' regime) was observed for U_a from 20m/s to 50m/s over the range of Re_f= 41-124. In this regime, the liquid film interface is covered by high frequency ripples and features a 'pebbled' surface, as describe by Hanratty (1957). According to the experimental results, the appearance of 3-D wavy surface could mainly attribute to the increase of airflow velocity, with the initial behavior of wave crests being irregular along transverse direction. Additionally, the characteristics of three-dimensional waves vary with experimental conditions. For a determined Re_f, with the increase of wind speed, larger individual ripple width and more curved ripple fronts were observed. Under the condition of an increasing Re_f at constant wind speed, one significant phenomena is the random coalescence of the single small ripple into relative large waves. The large wave occurs sporadically with limited width and height compared to large disturbance wave. When Re_f achieves certain value, large wave could appear in different

form, as marked in Figure 2(b), which indicates the gradual transition of '3-D wave' regime and disturbance wave regime.

(iii) 'Disturbance wave' regimeAt high liquid Reynolds numbers Re_f =165, and 207, the afore-mentioned 3-D waves would evolve into disturbance wave, also known as Kelvin-Helmholtz (K-H) wave. The disturbance wave regime is marked by very large-amplitude waves rising clearly above the substrate with quite high frequency, as can be seen from Fig. 2(c). The disturbance waves have some distinct features. For example, those large-amplitude waves move really fast with big mass compared to the three-dimensional waves at the same wind speed. It is noteworthy that ripples in between usually move quite slowly, which can be explained by momentum conservation. Besides, the wave fronts are covered by fast ripples and droplet entrainment usually occurs at the head of the waves in various form. Similar phenomenon is also described by Andrey et al. (2014). In this regime, the mixing of two phase flow is obvious, in the form of liquid droplets entrained into airflow or air entrained into liquid film as bubbles. Typical droplets entrainment results are demonstrated in Fig. 2(c).

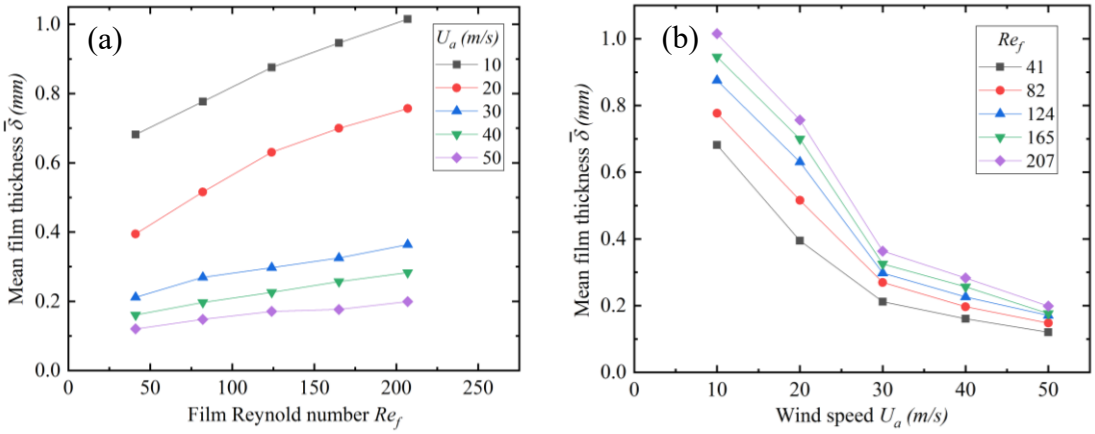

Figure 3: Mean film thickness $\bar{\delta}$ as a function of: (a) film Reynolds number Re_f, and (b) wind speed U_a

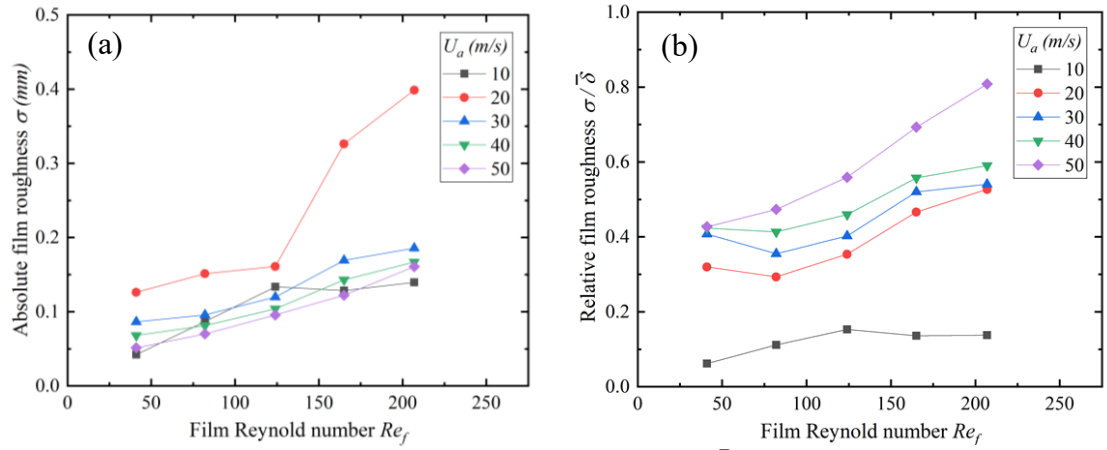

Figure 4: (a) Absolute roughness σ, and (b) relative roughness $\sigma/\bar{\delta}$ of the liquid film as a function of film Reynolds number Re_f for various wind speed U_a

3.2. Film thickness statistics

The mean film thicknesses $\bar{\delta}$ as a function of the film Reynolds number and wind speed, are shown in Fig. 3, respectively. Generally, the mean film thickness increases with increasing Re_f, and decrease with increasing U_a. Specifically, with Re_f remain unchanged, the rate of thickness growth decreases with the increase of wind speed. This may attribute to the acceleration of the flow within the liquid film due to the shear forces, or by the onset the liquid entrainment (Zadrazil et al. 2014). Note that the dramatically decrease is consistent with the transition from 2-D waves to 3-D waves.

The absolute ($\bar{\sigma}$) and relative ($\bar{\sigma}/\delta$) liquid film roughness as a function of Re_f are shown in Fig. 4, respectively. The absolute film roughness, which is the standard deviation of the liquid film thickness, show two distinctive trends.(i) For a constant Re_f, the absolute film roughness increases initially with increasing wind speed, reaches a maximum around U_a=20m/s, and then decrease again. (ii) When $U_a$is above 30m/s, $\bar{\sigma}$ increases gradually with increasing Re_f. A derivation of sudden increase can be seen at U_a=20m/s, Re_f=165, which may due to the wave regime change from 3-D waves to disturbance waves. The relative film roughness could reflect the fluctuation intensity better because the influence of the mean liquid film thickness is taken into account. Generally, the intensity of fluctuation increases with the increase of wind speed. The greatest interfacial fluctuations occur in the disturbance wave regime. In '2-D wave' regime, the relative roughness is small. The transition to 3-D waves is indicated by a sudden increase of the relative roughness. Similar increase happens when U_a change from 40m/s to 50m/s in 'disturbance wave' regime, which can attribute to the increasing frequency of disturbance waves. Evidence can be found in Section 3.3.

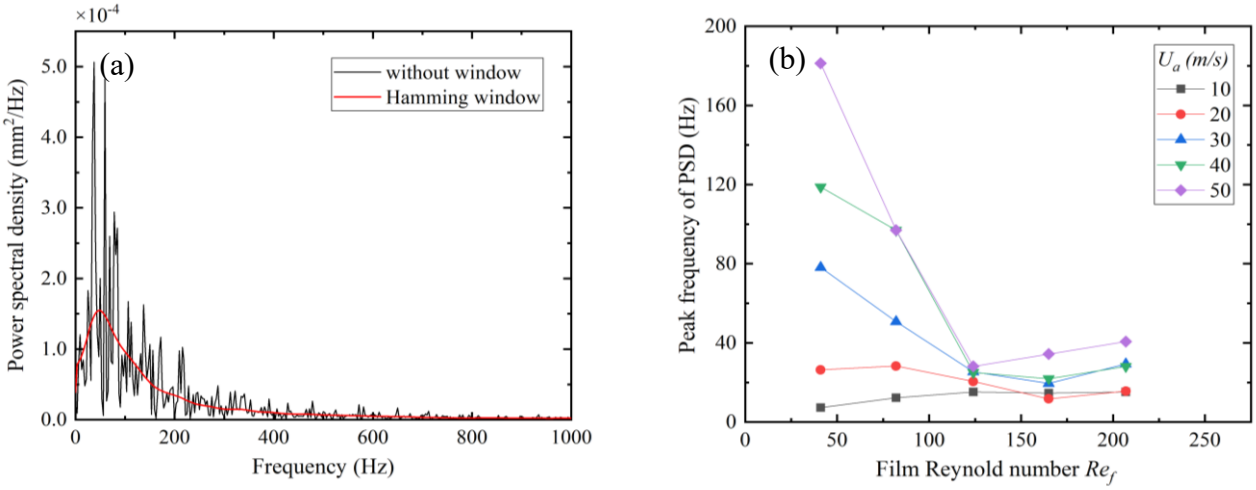

Figure 5: (a) Sample of Power spectral density (PSD) for U_a=50m/s, Re_f =208, and (b) Peak frequency of PSD as a function of film Reynolds number Re_f.

3.3 Wave statistics

The interfacial wave characteristics are investigated through a power spectral density (PSD) analysis. The PSDs are constructed from temporal film thickness time-traces. Sample results are graphed in Fig. 5(a), including the raw results and the results processed with Hamming window. It is accepted the peak of PSD represents the frequency of waves that carry the highest amount of energy (Leng et al. 2018). The maximum power frequency extracted from PSD results of current experiments is shown in Fig. 5(b) as a function of Re_f. It can be seen that the peak power frequency increases with increasing wind speed, which denotes the increase of surface fluctuations intensity. While for a constant U_a between 30m/s and 50m/s, the trend line descends first and then goes up with the increase of Re_f. The turning point can be recognized as the transition between '3-D wave' regime and 'disturbance wave' regime. More specifically, in the former regime, the high frequency ripples dominates the interface. With the increase of Re_f, those small ripples merges randomly to form large waves, which is revealed as a decrease of peak frequency. When the disturbance waves start to carry the highest amount of energy, their frequency tend to increase with increasing Re_f, thus a rise trend forms. And since the mass and velocity of disturbance waves are far greater than 3-D waves, the peak frequency of disturbance wave regime is reasonably lower in comparison. In the 2-D wave regime, the peak frequency increase slightly with increasing Re_f and eventually maintain an almost constant value.

4 Conclusion

A non-intrusive flow measurement technique, namely PLIF, was used for the detail characterization of the liquid film driven by high speed airflow pertinent to aircraft icing. Three distinct wave regimes were

identified based on qualitative observation and temporal film thickness time-traces. Additional quantitative analysis about interface roughness and wave characteristics were conducted to investigate the microphysics about liquid film. Two-dimensional waves were observed at wind speed U_a=10m/s with a sinusoidal feature. With the increase of film Reynolds number Re_f, the wave crests started to curve and the transition to three-dimensional waves happened. For U_a=20-50m/s, three-dimensional waves appeared at relative low Re_f ranging from 41 to 127. In this regime, the interface was covered by high frequency ripples with no obvious large wave appeared. When the Re_f reached above 165, the large amplitude disturbance waves, with quite high velocity, started to dominate the liquid film interface, accompany with frequent droplet entrainments. The wave regime transition was a gradual process from direct observation and film thickness time-traces. While for quantitative analysis (i.e., the peak frequency of the power spectral density), the transition between 'three-dimensional wave' regime to 'disturbance wave' regime was expressed visually by a turning point.

Acknowledgements

This work was financially supported by National Science Foundation of China under Grants No. 11672024 and 11372026 and National Basic Research Program of China under Grants No. 2015CB755803.

References

Olsen, W., & Walker, E. (1986). Experimental evidence for modifying the current physical model for ice accretion on aircraft surfaces.

Myers, T. G., & Thompson, C. P. (2015). Modeling the flow of water on aircraft in icing conditions. *Aiaa Journal*, 36(6), 1010-1013.

Liu, Y., Chen, W. L., Bond, L. J., & Hu, H. (2017). An experimental study on the characteristics of wind-driven surface water film flows by using a multi-transducer ultrasonic pulse-echo technique. *Physics of Fluids*, 29(1), 012102.

Zadrazil, I., Matar, O. K., & Markides, C. N. (2014). An experimental characterization of downwards gas–liquid annular flow by laser-induced fluorescence: flow regimes and film statistics. *International Journal of Multiphase Flow*, 60(2), 87-102.

Zhang, K., & Hu, H. (2015). An Experimental Study on The Transient Behavior of Wind-Driven Water Runback over a Flat Surface. *Aiaa Aerospace Sciences Meeting*.

Leng, M., Chang, S., & Wu, H. (2018). Experimental investigation of shear-driven water film flows on horizontal metal plate. *Experimental Thermal & Fluid Science*, 94.

Schubring, D., Ashwood, A. C., Shedd, T. A., & Hurlburt, E. T. (2010). Planar laser-induced fluorescence (plif) measurements of liquid film thickness in annular flow. part I: methods and data. *International Journal of Multiphase Flow*, 36(10), 815-824.

Hanratty, T. J., & †, J. M. E. (1957). Interaction between a turbulent air stream and a moving water surface. *Aiche Journal*, 3(3), 299–304.

Cherdantsev, A. V., Hann, D. B., & Azzopardi, B. J. (2014). Study of gas-sheared liquid film in horizontal rectangular duct using high-speed lif technique: three-dimensional wavy structure and its relation to liquid entrainment. *International Journal of Multiphase Flow*, 67, 52-64.

Gent, R. W., Dart, N. P., & Cansdale, J. T. (2000). Aircraft icing. Philosophical Transactions Mathematical Physical & Engineering Sciences, 358(1776), 2873-2911.